

# High resolution spectral self-interference fluorescence microscopy

Anna K. Swan<sup>1</sup>, Lev Moiseev<sup>2</sup>, Yunjie Tong<sup>3</sup>, S. H. Lipoff<sup>4\*</sup>, W.C. Karl, B.B Goldberg<sup>3</sup>, M.S. Ünlü<sup>3</sup>, Boston University, <sup>1</sup>Dept of Electrical and Computer Engineering, <sup>2</sup>Department of Biology, <sup>3</sup>Department of Physics, <sup>4</sup>Boston University Academy.

## ABSTRACT

We present a new method of fluorescence imaging, which yields nm-scale axial height determination and ~15 nm axial resolution. The method uses the unique *spectral* signature of the fluorescent emission intensity well above a reflecting surface to determine vertical position unambiguously. We have demonstrated axial height determination with nm sensitivity by resolving the height difference of fluorescein directly on the surface or on top of streptavidin. While different positions of fluorophores of different color are determined independently with nm precision, resolving the position of two fluorophores of the same color is a more convoluted problem due to the finite spectral emission width of the fluorophores. Hence, for physically close ( $<\lambda/2$ ) fluorophores, it is necessary to collect multiple spectra by independently scanning an excitation standing wave in order to deconvolute the contribution to the spectral pattern from different heights. Moving the excitation standing wave successively enhances or suppresses excitation from different parts of the height distribution, changing the spectral content. This way two fluorophores of the same color can be resolved to better than 20 nm. Design aspects of the dielectric stack for independent excitation wave scanning and limits of deconvolution for an arbitrary height distribution will be discussed.

**Keywords:** Fluorescence microscopy, self-interference, spectroscopy

## 1. INTRODUCTION

The advantage of light microscopy over electron and scanned probe microscopy is the ability to image the interior of biological specimens. Light would be an ideal carrier of microscopic information if it weren't for the resolution limit. But because of diffraction, standard light microscopes are not able to discern two objects closer together than about 200 nm in the focal plane. In the direction perpendicular to the focal plane, the resolution is worse, about 600 nm. There is an impressive body of work under way where the optical resolution is constantly incrementally improved. The greater resolution originates from several general approaches. Higher resolution for all types of light microscopy will be achieved by collecting a significantly larger numerical aperture. Specific to fluorescence microscopy, modulation of standing waves of the excitation optical field in the axial and lateral directions can be used for higher resolution. Recent advances in light microscopy have pushed the limits of resolution of optical microscopy down to just below 100 nanometers.<sup>1</sup> Use of two large aperture objectives results in collection of the maximum solid angle in 4Pi-confocal microscopy.<sup>2</sup> As a beautiful example, sub-100 nm resolution has been achieved by combining 4Pi-confocal microscopy with subsequent image restoration<sup>3</sup>. Fluorescence microscopy by standing-wave excitation<sup>4</sup> exploits interference in the excitation optical field to create a periodic modulation. Scanning the standing wave, collecting fluorescence and subsequent deconvolution<sup>5,6</sup> also yields sub 100 nm axial resolution, and has been further extended in the lateral direction.<sup>7</sup> Combining wide field collection with interference in the emission plus the excitation leads to fM.<sup>8</sup> Also, by exploiting characteristics unique to fluorescent probes, stimulated emission has been used to quench the fluorescence *surrounding* a very small volume, thus effectively increasing the resolution in both lateral and axial directions to ~100nm.<sup>9</sup> However, using light and achieving nanoscale resolving power is still out of reach.

It is important here to make a clear distinction between resolution and the precise location determination of a single source. Resolution is the ability to resolve two nearby points as distinct and can be applied to arbitrary distributions, while single source position determination will only average the position of closely spaced objects. Position determination of a single source is routinely achieved with nanometer precision using light interference, and is often loosely referred to as nanometer resolution.

In this paper we demonstrate the ability to use light interference to determine location with nanometer precision and discuss how by combining it with spectral information and scanning excitation standing wave to achieve not only precise localization of a single source, but nanoscale *resolution*. With spectral self-interference, the individual fluorophore height information is encoded in the measured spectrum, and the height distribution of the fluorophores is revealed through deconvolution of the spectrum. To remove degeneracy between alternative fluorophore

distributions, the excitation standing wave is scanned and a set of spectra collected. Initial simulations indicate that sources spaced 14 nm apart can be resolved, so that *optical resolution* can be brought in to the nanoscale regime for the first time.

## 2. INTRODUCTION TO SPECTRAL SELF-INTERFERENCE

For many years scientists have recognized that fluorophores are often quenched when they are placed upon surfaces. Mechanisms of energy transfer, standing wave nodes in the excitation field, and destructive interference in the emission all lead to significant reductions in fluorescence. Ten years ago, Fromherz and co-workers noted that the intensity of the total fluorescence oscillates as a function of the fluorophore height above a reflecting substrate<sup>10</sup>. Building upon work performed many years ago by Drexhage<sup>11</sup> they utilized a convolution of the excitation standing wave and emission interference to sensitively locate the vertical position of the fluorophore in close proximity to a reflecting surface. Because the fluorophore is within  $\sim\lambda$  of the reflecting surface, the entire spectrum of the emission is quenched or enhanced as the light undergoes constructive and destructive interference as a function of the vertical distance. Fromherz's method is based on measuring the intensity of the fluorophore for several known silicon dioxide heights in order to determine the height of the fluorophore above the dioxide layer.

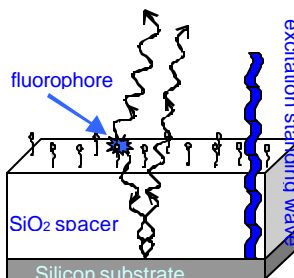


**Fig. 1** A thick, transparent SiO<sub>2</sub> layer is used as a spacer between the fluorescent markers and the primary mirror surface (Si/SiO<sub>2</sub> interface) to create spectral oscillations in the emission signal. Excitation standing wave also shown

Spectral self-interference fluorescence microscopy is different in that the separation between the fluorophore and the reflecting substrate is much greater, on the order of 10-15 wavelengths. The longer path length difference between the direct and reflected light means only a small change in wavelength is needed to go between constructive and destructive interference. The result is *spectral* oscillations, or fringes, in the spectrum – a unique signature of the height of the emitter. Small height differences produce shifts in the fringes and changes in the period of oscillation (the latter are less noticeable). If the fluorescent markers are at a prescribed distance from the surface, the resulting spectrum can be calculated. Inversely, the distance above the mirror can be determined solely from the oscillations within the spectrum. Unlike fluorescence interference-contrast microscopy, it should be noted that as the height information is encoded in the spectrum, our approach is independent of the fluorophore density, emission intensity, and the excitation field strength.

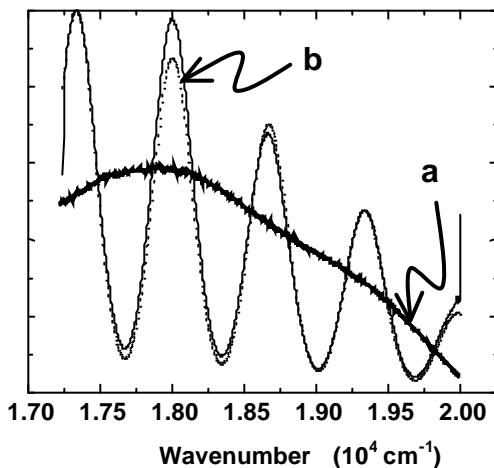


**Fig. 2** (a) Spectrum,  $I_{em}(\lambda^{-1})$  of a monolayer of fluorescein on a microscope slide, measured with a 50X objective. (b) Spectrum from a monolayer of fluorescein atop a 5.052  $\mu\text{m}$  SiO<sub>2</sub> spacer on a Si mirror. Solid line-measured spectrum, dashed line-fit. 5X objective used.

In Figure 1 we display a fluorophore located atop a thick SiO<sub>2</sub> spacer layer on top of silicon, the main reflecting surface. The figure illustrates both the direct and reflected emitted light paths that cause interference. The effect of introducing a reflecting surface at such a large separation is demonstrated in Fig 2. by measuring the emission from a monolayer of fluorescein on a glass microscope slide as compared to the spectrum of a monolayer of fluorescein on a 5.052  $\mu\text{m}$  thick SiO<sub>2</sub> layer atop a silicon substrate that acts as a mirror. Note the standard smooth spectrum in Fig. 2a is greatly modified with several large contrast fringes in Fig. 2b. The intensity peaks and valleys in Fig. 2b correspond to conditions where the height difference from the reflected path interferes constructively or destructively with the direct light (Fig.1). The thin dotted line is a calculated spectrum fit to the data based upon our model described below. The spectrum in Fig 2b has an envelope that reflects the overall emission spectrum shape of 2a. The excitation field intensity simply scales the emission intensity of the spectrum. Similarly, the fluorophore density can also scale the spectrum intensity. However, neither simple scaling modifies the phase or period information of the spectral oscillations.

## 2.2 Analysis of self-interference

The collected spectrum can be inverted to obtain the fluorophore height distribution if the material parameters of the reflecting dielectric stack are known. Since we are fabricating a material system with well-known spatial and dielectric properties, we can determine the fluorophore height distribution without any adjustable parameters. The spectrum is composed of three different components, two of which only scale the overall intensity of the fluorescence emission spectrum -- the excitation intensity and the spectrum envelope. The third component creates the spectral fringe pattern that holds all of the height information. The fringe pattern is given by the interference of the emission with its reflection from the mirror. The interference component of the intensity for each emitter is given by:

$$\left| 1 + r e^{-i k_0 2(nD+d)} \right|^2 = 1 + r^2 + 2 r \cos(k_0 2(nD + d))$$

Here,  $r$  is the total reflectivity of the mirror-system,  $nD$  is optical path in the  $\text{SiO}_2$  spacer layer, which is measured independently by white light reflectivity measurement. The fringes in the white light spectrum reflect the cavity given by  $nD$ . The only unknown is  $d$ , the height of the emitter above the surface. Thus the fluorophore creates a unique spectrum. The sub-nanometer sensitivity is demonstrated in Fig. 3, where the measured spectrum is divided by the calculated spectrum and a simple least-squares fitting procedure yields  $\pm 0.5\text{nm}$  precision in the height of the fluorophores  $D$ .

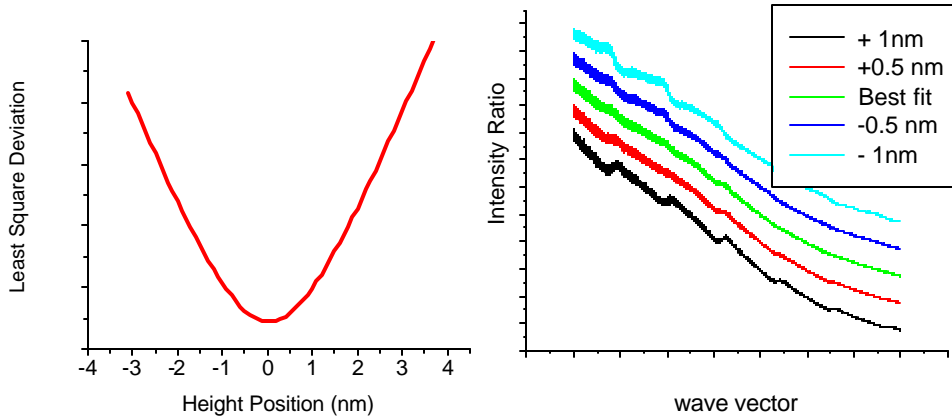


**Fig. 3.** Illustration of sub-nm sensitivity in fitting of the height. **Fig. 3a)** Least square deviation from smooth curve fit with a minimum at 5098.2 nm. **Fig. 3b)** shows the ratio of measured data with fitted spectrum and yields a smooth fluorescence envelope when  $D$  is correct. The difference in  $D$  is  $\pm 0.5\text{ nm}$  and  $\pm 1\text{nm}$  for the non-smooth curves

## 2.3 Experimental setup

All of the samples presented here were prepared on silicon chips with a  $\sim 5\ \mu\text{m}$  thick  $\text{SiO}_2$  layer on top to provide both reflection (primarily from the  $\text{SiO}_2/\text{silicon}$  interface) and a spacer layer thick enough to provide 4-5 fringes in the fluorescence spectrum. A Renishaw 1000B Raman Spectrometer supplies the excitation and collection optics with a single monochromator and a thermoelectrically cooled charge coupled device (CCD) used for light collection. A Leica LM/DM microscope with a high precision ( $0.2\ \mu\text{m}$ ) motorized stage is used for confocal light collection and scanning of the sample. Fluorescein has been used as the fluorophore in all experiments. An Ar Ion laser with  $\lambda = 488\ \text{nm}$  has been used for excitation of the fluorophore. Spectra have been collected between 500-600 nm. When using a planar mirror for interference microscopy, one has to collect the light using an objective with small collection angle. Otherwise the optical path length varies greatly as angles away from surface normal are summed. In spectral self-interference, this has the effect of blurring the spectral information with eventual complete loss in fidelity. Because of this effect, we have used an objective with low numerical aperture (NA) in preliminary experiments. With a 5X objective of  $NA=0.12$ , the problem of path-averaging is minimal.

### 3. UTILIZATION OF SPECTRAL SELF-INTERFERENCE FOR MICROSCOPY

#### 3.1 Height determination from a wedge using spectral information

The simplest demonstration of spectral self-interference is illustrated in Fig. 4, where we have used a wedge structure to easily vary the height of the fluorophore above the reflecting surface. A shallow wedge of SiO<sub>2</sub> atop silicon with an aspect ratio of 125 nm height per mm translation was made by slow immersion into a HF etch bath. With such a small aspect ratio, even a relatively large spot size of ~3 μm causes a height variation of only ±0.2 nm for the spectrum at each position. The wedge was covered with a monolayer of fluorescein immobilized on the surface. The 488nm line of an Ar<sup>+</sup>-ion laser was used for excitation and the resulting emission spectrum was measured between 500 and 580 nm (20 000-17240 cm<sup>-1</sup>). Seven successive spectra are shown in Fig. 4, each measured from a different lateral position along the wedge that corresponds to an increase in fluorophore-to-reflector separation of 12.5 nm per step. As expected, the peaks move toward lower wave numbers as the height increases. The wafer used was actually a waveguide and so included a layer of Si<sub>3</sub>N<sub>4</sub> that caused additional reflections, producing an envelope that differed from the usual fluorescein fluorescence intensity envelope. The spectra are modeled using the complete known dielectric structure, which reproduces not only the peak positions, but also the envelope shape.

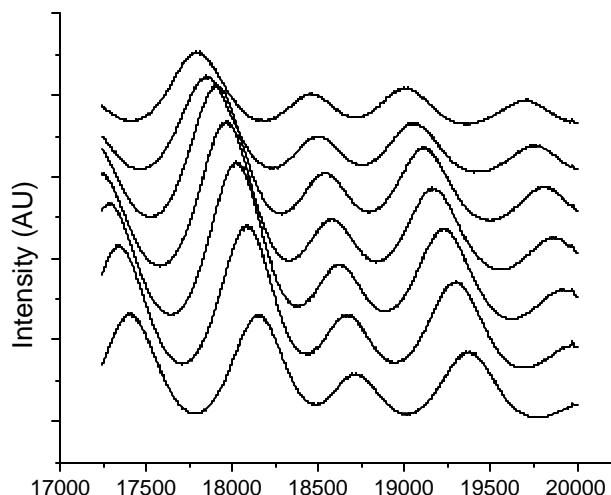


**Fig. 4.** Successive spectra from a shallow wedge structure. Each spectrum is measured from a lateral position that corresponds to an increase in fluorophore to reflector separation of 12.5 nm. Spectra moves towards lower wavenumber as height increases. The spectra are offset vertically for clarity.

#### 3.2 Resolving the height of a 5 nm globular protein

We have applied spectral self-interference fluorescence microscopy to measure the height difference between a fluorescent marker immobilized directly atop a substrate and one immobilized also atop of a globular protein<sup>12</sup>. We used streptavidin-C. Each of the four subunits of this globular protein contains a cysteine-terminated tail, two of which can be used to immobilize the protein on surfaces via sulfhydryde-reactive crosslinkers, leaving two sulfhydryde groups unreacted and available for further immobilization. Fluorescein maleimide was attached to these groups to form a fluorescent monolayer on top of the streptavidin film on the SiO<sub>2</sub>/Si substrates. Half the chip is covered with fluorescein directly immobilized on the SiO<sub>2</sub> surface and the other half is covered with a monolayer of streptavidin with fluorescein on top. Spectra from the two areas are clearly differentiated as shown in Fig. 5. An analysis of our measurements yields optical path length differences of 5 to 8 nm between the areas. This result agrees well with the known size of the protein (~5nm).

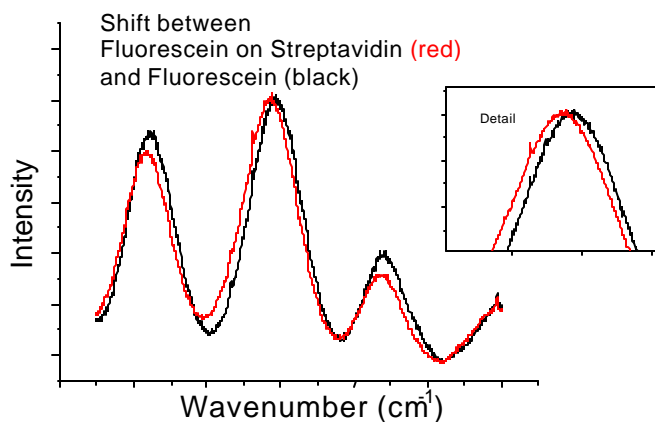


**Fig. 5.** Comparison of spectra obtained from fluorescein bound on top of a monolayer of streptavidin vs. that directly bound on the underlying substrate.

### 3.3 Resolving a nanometer scale height in an artificial fluorescent structure

Using spectral self-interference, we have determined the vertical height of fluorophores bound to a silicon dioxide surface. The sample was prepared by reactive ion etching of a 12nm step edge into a 5  $\mu\text{m}$  thick thermal oxide grown atop a silicon wafer. The silicon/silicon dioxide interface acts as a reflector for the self-interference. The spectra are collected by a scanning the microscope stage, and the data analyzed using the model discussed above. Figure 6 displays the height data as a false color image, where it is apparent that nanometer vertical resolution is obtained. Note that this is *not* the fluorescence intensity, which is relatively uniform. Rather, this image displays the height of the fluorophores as determined by the spectral self-interference.

It is worth mentioning again that there are no adjustable parameters in the fitting since we are using the complex reflectivity  $r$ , which is calculated solely based on the known material parameters of the substrate.

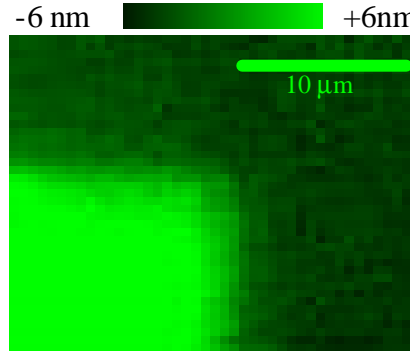


**Fig. 6.** Spectral self-interference image of fluorescein on a step-etched silicon oxide layer atop silicon. The color corresponds to the height of the fluorescent emitter, the actual intensity is uniform. The image demonstrates nm scale resolving power of the spectral self-interference technique.

### 3.4 Measuring polarization of fluorescein tagged ssDNA

Little is known about the conformation of single stranded (ss) DNA immobilized on a surface. However this is of great interest when developing DNA-based arrays<sup>13</sup>. A DNA strand, which is attached to the surface at one end, will have different probability of forming a double-stranded (ds) DNA helix with a matching sequence, depending on whether the ssDNA is laying on the surface or is extended out in solution, the latter being more favorable for dsDNA formation. A surface covered with amino-silane is electrically charged at normal pH and hence the charged ssDNA tend to stick to the surface. With enough screening provided by a high-salt and pH solution, the free end of the DNA should be extended in the solution. We have been using fluorescein tagged 20mers and 50mers to explore the confirmation using spectral self-interference. However, it has proved more difficult than anticipated to make the free ends detach. In this process we found that the fluorescence signal appeared to come from below the SiO<sub>2</sub>/ water interface, clearly an unphysical result. Our tentative explanation is that this apparent discrepancy is due to an average non-zero polar angle orientation of the dipole and modeling is under way.

## 4 VERTICAL RESOLUTION OF TWO OR MORE SOURCES

The primary limitation with the current configuration is that we have only determined the vertical position of a single layer, which is *not* resolution. While different positions of fluorophores of different color are determined independently with nm precision, just as for a single source, resolving the position of two fluorophores of the same color is a more convoluted problem due to the finite spectral emission window of the fluorophores. Below we will discuss how to achieve nanoscale *resolution* of two or more sources distributed arbitrarily along the optical axis.

### 4.1 Nanometer resolution of two closely spaced independent sources

As demonstrated above, we have a good understanding of how to precisely determine the vertical height position from a single layer encoded by self-interference into the measured spectrum. Here we will discuss the principle for resolving two closely spaced layers of fluorophores of the same color.

Consider two otherwise identical fluorescent sources at two different heights. Since the intensity contributions from two incoherent sources are added,  $I \propto \sum A_i^2 [1 + R^2 + 2R \cos(2k(nD + d_i))]$ . In this case the sum has two terms. The two sources generate a new cosine where the frequency is determined by the average height of the pair, modulated by the difference in height. For an infinite frequency range, one could, in principle, resolve minute difference through the beating of the envelope function and via Fourier analysis resolve arbitrarily close fluorophores. However, the emitters only provide a limited frequency window or bandwidth, and with the typical spectral emission window of  $\sim 100\text{nm}$ , the smallest separation that can be readily detected is limited to  $\sim \lambda/4$ . Clearly, this is not nanometer axial resolution. However, by combining the spectral information together with a vertical sweep of the standing excitation wave, a recent technique used for vertical and lateral resolution enhancement true resolution can be restored to the precision of a single height determination. Since the spectrum is the incoherent sum of the two, the spectral peak

position will be weighted according to the excitation field intensity located at each fluorophore position, causing a fringe shift in the total spectrum as the excitation standing wave is scanned. Hence, by scanning the excitation standing wave relative to the fluorophore distribution, two sources can be resolved to near nm resolution (albeit with longer collection times) In the sections below, discuss how to implement scanning of the standing wave, followed by an analysis of how to deconvolve the signal not only from two sources, but from an arbitrary vertical distribution. by using the combination of standing wave scanning and spectral self-interference with mathematical inversion methods.

#### 4.2 Design and fabrication of dielectric mirror stack for independent scanning of the excitation wave

For self-interference spectroscopy the sample must be separated from the mirror by many wavelengths, which requires a buried reflector. While a mirror at a fixed depth ( $\sim 5 \mu\text{m}$ ) is used for the self-interference, a moving mirror is desired to be able to scan the standing wave formation at the excitation wavelength. Hence, the first mirror will have to reflect the emission wavelengths and be transparent at the excitation wavelength. A separate movable mirror reflects the excitation wavelength and allows for scanning the excitation standing wave through the fluorophore distribution.

The challenge in building the functionality described above lies in designing a dielectric mirror with uniformly high reflectivity through a range of wavelengths corresponding to the emission spectrum combined with transparency at the excitation wavelength. This is not a novel problem, since dielectric mirror stacks with alternating layers of quarter wavelength thick dielectric materials with different refractive indices are used in many optical and photonics applications. For example, the design of reflectors with a low-reflection optical window is an important feature for optically pumped vertical-cavity surface-emitting lasers (VCSELs)<sup>14</sup> Our design and simulation techniques on this type of VCSELs<sup>15</sup> on and Resonant Cavity Enhanced (RCE) photodetectors,<sup>16</sup> are easily adapted for fluorescence self interference.

For the wavelengths of fluorescent tags commonly used in biology, Si compatible materials such as  $\text{Si}_3\text{N}_4$ ,  $\text{SiO}_2$ , and a continuous composition of  $\text{SiO}_x\text{N}_y$  provides sufficient flexibility to design mirrors with ample spectral stop band for the emission wavelengths as well as a window of low reflectance for the optical excitation. The well-established fabrication capabilities on Si substrates allow for developing compact and potentially inexpensive MEMS based devices for independent excitation wave scanning.

#### 4.3 Reconstruction of arbitrary 1D vertical distribution for nanometer resolution

It is a major data inversion problem to take a spectrum comprised of contributions from many independent sources along the vertical direction to reconstruct the vertical fluorescence distribution. The steps of this process are similar in spirit to the demodulation steps of synthetic aperture radar (SAR) imaging, where high range resolution is obtained.

We use the model of the observation process based on the physical properties of the system described above and then use this model as the basis for inversion. The unknown distribution of fluorophores as represented by the profile  $A(d)$  is first discretized into a series of axial slices at heights  $d_i$  to obtain a discrete set of unknowns  $A_i$ . These unknown amplitudes corresponding to each slice are then determined from the set of spectra measured as the standing wave is scanned. Such a measured spectrum can be written in the following form:

$$(1) \quad S_j = \sum_{i=1}^N I_j(d_i) A_i^2 \left[ 1 + R^2 + 2R \cos(2k(nD + d_i)) \right] = \sum_{i=1}^N I_j(d_i) A_i^2 F_i$$

where  $F_i$  is the interference term,  $I_j(d_i)$  is the strength of the excitation intensity at height  $d_i$  for standing wave position  $j$  (which we will scan), and  $S_j$  is the entire observed spectrum and  $A_i$  is the emission amplitude to be determined from position  $d_i$ . Here we have normalized the spectra by  $I_m(k)$  (see Fig. 1a). We want to find the  $N$  unknown amplitudes  $A_i$ . If we move the excitation field to a different position, the resulting spectrum is

$$S_{j+1} = \sum_{i=1}^N I_{j+1}(d_i) A_i^2 F_i.$$

Collecting the observations from  $N$  different excitation-field position measurements yields the matrix equation

$$(2) \quad \begin{bmatrix} S_1(k) \\ S_2(k) \\ \vdots \\ S_N(k) \end{bmatrix} = \begin{bmatrix} I_1(d_1)F_1 & I_1(d_2)F_2 & \cdots & I_1(d_N)F_N \\ I_2(d_1)F_1 & I_2(d_2)F_2 & \cdots & I_2(d_N)F_N \\ \vdots & \vdots & \ddots & \vdots \\ I_N(d_1)F_1 & I_N(d_2)F_2 & \cdots & I_N(d_N)F_N \end{bmatrix} \begin{bmatrix} A_1^2 \\ A_2^2 \\ \vdots \\ A_N^2 \end{bmatrix}$$

Or in shorthand;

$$(3) \quad \underline{\mathbf{S}} = \underline{\mathbf{C}} \underline{\mathbf{A}}$$

Equation (3) governs the inverse problem of recovering the unknown but desired depth emission profile specified by the numbers  $A_1^2, A_2^2, \dots, A_N^2$ . Note that this system of equations is in general not square, since each  $S_i(k)$  represents a vector of observations. In addition to the observation model captured in (3), in practice there are sources of noise and uncertainty. Thus, a better model of the observation process is given by:  $\underline{\mathbf{S}} = \underline{\mathbf{C}} \underline{\mathbf{A}} + \underline{\mathbf{w}}$  where  $\underline{\mathbf{w}}$  represents additive noise or perturbation. Note that this model involves a weighted summing operation or projection onto the rows of the  $S_j$ . Thus the data are generalized Fourier observations. Such inverse problems are known to be ill-posed and must be solved with care. The relative difficulty in solving this linear inverse problem is related to the properties of the observation matrix  $\underline{\mathbf{C}}$ . For example, the condition number<sup>17</sup>  $\kappa(\underline{\mathbf{C}})$  of  $\underline{\mathbf{C}}$  gives a measure of the sensitivity of the solution of the set of equations to perturbations in both  $\underline{\mathbf{C}}$  and  $\underline{\mathbf{S}}$ . Further, the structure of  $\underline{\mathbf{C}}$ , as revealed through analyses such as the singular value decomposition, yields information about the robustness of the problem to inversion and determines the resolution limit in the presence of noise. Initial inversions without inclusion

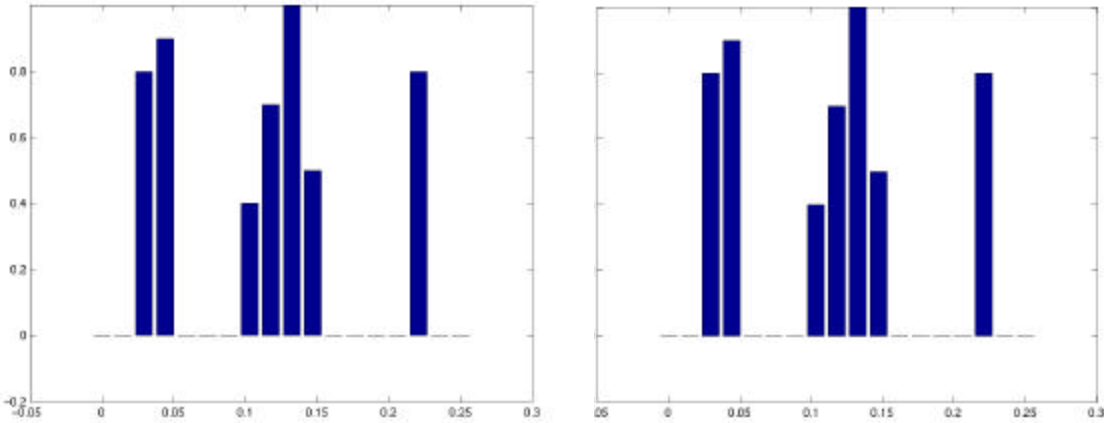


**Fig.7** The constructed arbitrary fluorophore distribution to the left is used to generate spectral data for 8 different scanning excitation wave positions spanning  $\pm \lambda_{ex}/4$ . ( $\lambda_{ex}=488\text{nm}$ ) These spectra are subsequently used for data inversion according the model discussed. The bin size used is 14 nm steps which is large enough for the inversion, shown to the right, to deliver the initial fluorophore distribution, shown to the left. Here noise is not included.

of any prior knowledge (e.g. no restriction to positive amplitudes) shows that spectra from a distribution consisting of three groups of fluorescence sources, spaced 14 nm apart over 250 nm height can be accurately inverted as demonstrated in Fig 7. The constructed arbitrary fluorophore distribution is used to generate spectral data for 8 different scanning excitation wave positions spanning  $\pm \lambda_{ex}/4$ . ( $\lambda_{ex}=488\text{nm}$ ) These spectra are subsequently used for data inversion according the model discussed. The bin size used is 14 nm wide steps that are large enough for the inversion to deliver the initial fluorophore distribution. Here noise is not included, which if included would make the inversion less stable and limit resolution. We are working on the limits of resolution for given levels of system noise and given numbers of observations. In particular, the required data acquisition (e.g. the number of experiments to perform parameterized by the number of discrete standing wave positions to collect) so the resulting estimated concentration profile is valid.

Further, we may combine the observation equation in (3) with prior knowledge concerning the emission profile to regularize the problem. The application of such regularization methods can stabilize the solution even in those cases where the physical observations still result in sensitive inversion problems. For example, if we know that the  $A_i$

change smoothly with depth, we can enforce this knowledge on the solution and make the solutions more robust in the presence of noise or data loss. Alternatively, if we know that the fluorophore distribution is sparse for a given application, this information can be used to focus the noisy data and improve resolution. We have had good success incorporating such prior information in model-based approaches to SAR image reconstruction and other inverse problems<sup>18,19,20</sup>.

## 5 CONCLUSIONS

We have introduced a novel method of achieving nanometer height determination capability that is totally independent from fluorophore concentration or excitation field strength, building upon earlier work by Drexhage and Fromherz. The technique utilizes self-interference between directly collected and reflected light, emitted many wavelengths above a buried reflector. The resulting unique spectral signature is analyzed using known material parameters to find the vertical position of the fluorophore with sub-nanometer precision. More importantly, we suggest that optical resolution on the order of 10-20 nm can be achieved by independently scanning the excitation standing wave and invert the result to reveal the vertical fluorescence distribution. Initial calculations show that in absence of noise, 14 nm resolution can be achieved. This represents a factor of five improvement of the current state-of-the-art in optical resolution.

---

<sup>1</sup> M. G. L. Gustafsson, "Extended resolution fluorescence microscopy," *Biophysical Methods* 627 (1999).

<sup>2</sup> S. W. Hell, E. H. K. Stelzer, "Properties of a 4Pi confocal fluorescence microscope," *J. Opt. Soc. Am. A*, **9** 2159 (1992); S. W. Hell, E. H. K. Stelzer, S. Lindek, and C. Cremer, "Confocal microscopy with an increased detection aperture: type-B 4Pi confocal microscopy," *Opt. Letters* **19** 222 (1994); M. Schrader, K. Bahlmann, G. Giesse and S. W. Hell, "4Pi-Confocal Imaging in Fixed Biological Specimens," *Biophysical Journal* **75**, 1659 (1998).

<sup>3</sup> S. W. Hell, S. Lindek, C. Cremer, and E. H. K. Stelzer, *Appl. Phys. Lett.* **64**, 1335 (1994) "Measurement of the 4Pi-confocal point spread function proves 75 nm axial resolution"

<sup>4</sup> B. Bailey, D. Farkas, D. L. Taylor, and F. Lanni, "Enhancement of axial resolution in fluorescence microscopy by standing-wave excitation," *Nature*, **366**, 44 (1993).

<sup>5</sup> V. Krishnamurthi, B. Bailey, and F. Lanni, "Image processing in 3-D standing-wave fluorescence microscopy," *SPIE* **2655**, 18 (1996).

<sup>6</sup> B. Schneider, J. Bradl, I. Kirsten, M. Hausmann, and C. Cremer in "High precision localization of fluorescent target in the nanometer range by spatially modulated excitation fluorescence microscopy," *Fluorescence Microscopy and Fluorescent Probes*, Vol 2 Slavik (ed) 62 (Plenum Press, New York, 1998).

<sup>7</sup> R. Heintzmann, C. Cremer, "Laterally modulated excitation microscopy: improvement of resolution using a diffraction grating," *Proc. SPIE* 3568: 185 (1998) and Peter So, MIT

<sup>8</sup> M. G. L. Gustafsson, D. A. Agard, and J. W. Sedat, "Seven-fold improvement of axial resolution in 3D widefield microscopy using two objective lenses," *Proc SPIE*, **2412** 147 (1995); M. G. L. Gustafsson, D. A. Agard, J. W. Sedat, "3D widefield light microscopy with better than 100nm axial resolution," *J. Microscopy* **195**, 10 (1998).

<sup>9</sup> T. Klar, S. Jakobs, M. Dyba, A. Egner, and S. W. Hell, "Fluorescence microscopy with diffraction barrier broken by stimulated emission," *PNAS*, **97** 8206 (2000); T. A. Klar, M. Dyba, and S. W. Hell, "Stimulated emission depletion microscopy with an offset depleting beam," *Appl. Phys. Lett.* **78**, 393 (2001).

<sup>10</sup> A. Lambacher and P. Fromherz, "Fluorescence interference-contrast microscopy on oxidized silicon using a monomolecular dye layer," *Appl. Phys. A* **63**, 207 (1996); D. Braun and P. Fromherz, "Fluorescence interference-contrast microscopy of cell adhesion on oxidized silicon," *Appl. Phys. A* **65**, 341 (1997); D. Braun and P. Fromherz, "Fluorescence Interferometry of Neuronal Cell Adhesion on Microstructured Silicon," *Phys. Rev. Lett.* **81** 5241 (1998).

<sup>11</sup> K. Drexhage, "Monomolecular layers and light" *Scientific American*, 6 108, 1970; K. H. Drexhage, "Interaction of light with monomolecular dye layers," *Prog Optics*. **12**, 163-232 (1974).

<sup>12</sup> A.K. Swan, M. S. Ünlü, Y. Tong , B.B. Goldberg, L. Moiseev and C. Cantor, "Self-Interference Fluorescent Emission Microscopy - 5nm Vertical Resolution" *Proceedings of CLEO* (2001).

<sup>13</sup> Chareyere, M-T., Tcherkasskaya, O., and Winnik, M.A. (1997) Fluorescence energy transfer study of the conformation of oligonucleotides covalently bound to polystyrene latex particles. *Langmuir*, **13**, 3103-3110.

<sup>14</sup> K. J. Knopp, D. H. Christensen, and J. R. Hill, "Vertical-cavity surface-emitting lasers with low-ripple optical pumping windows," *IEEE J. Select. Topics in Quantum Electron.*, Vol.3(2), pp. 366-371 (1997).

<sup>15</sup> G. H. Vander Rhodes, J. M. Pomeroy, M.S. Ünlü, B. B. Goldberg, K. J. Knopp, and D. H. Christensen, "Pump intensity profiling of vertical-cavity surface-emitting lasers using near-field scanning optical microscopy," *Appl. Phys. Lett.*, Vol. **72**(15), pp. 1811-1813, (1998).

<sup>16</sup> M. S. Ünlü and S. Strite, "Resonant Cavity Enhanced Photonic Devices," *Appl. Phys. Rev. J. Appl. Phys.*, Vol. **78**(2), pp. 607-639, (1995). (invited)

---

<sup>17</sup> Gene H. Golub and Charles F. Van Loan "Matrix Computations", *Johns Hopkins University Press* (1989)

<sup>18</sup> M. Cetin and W. C. Karl, "Feature-enhanced synthetic aperture radar image formation based on non-quadratic regularization," *IEEE Transactions on Image Processing*, **10**, pg. 623--631, 2001.

<sup>19</sup> M. Cetin and W. C. Karl, "Superresolution and edge-preserving reconstruction of complex-valued synthetic aperture radar images," *Proc. of the 2000 IEEE International Conference on Image Processing*, Vancouver, British Columbia, Canada, Vol. 1, pg 701--704, September 10-13, 2000.

<sup>20</sup> V. Galdi, W. C. Karl, D. A. Castanon, and L. B. Felsen, "Approaches to Underground Imaging for Object Localization," in *Detection and Remediation Technologies for Mines and Mine-Like Targets VI*, A. C. Dubey, J. F. Harvey, J. T. Broach, and V. George editors, Proc. SPIE V 4394, SPIE, Orlando, April 16--20, 2001.